

Memory effects and Lévy walk dynamics in intracellular transport of cargoes

Sergei Fedotov,¹ Nickolay Korabel,¹ Thomas A. Waigh,^{2,3} Daniel Han,^{1,4} and Victoria J. Allan⁴

¹*School of Mathematics, University of Manchester, Manchester M13 9PL, United Kingdom*

²*Biological Physics, School of Physics and Astronomy, University of Manchester, Manchester M13 9PL, United Kingdom*

³*The Photon Science Institute, University of Manchester, Manchester M13 9PL, United Kingdom*

⁴*Faculty of Biology, Medicine and Health, School of Biological Sciences, University of Manchester, Manchester M13 9PL, United Kingdom*



(Received 9 May 2018; revised manuscript received 10 July 2018; published 22 October 2018)

We demonstrate the phenomenon of cumulative inertia in intracellular transport involving multiple motor proteins in human epithelial cells by measuring the empirical survival probability of cargoes on the microtubule and their detachment rates. We found the longer a cargo moves along a microtubule, the less likely it detaches from it. As a result, the movement of cargoes is non-Markovian and involves a memory. We observe memory effects on the scale of up to 2 s. We provide a theoretical link between the measured detachment rate and the superdiffusive Lévy-walk-like cargo movement.

DOI: [10.1103/PhysRevE.98.042136](https://doi.org/10.1103/PhysRevE.98.042136)

I. INTRODUCTION

Intracellular transport of cargoes along microtubules is a classical example of active transport [1,2]. It is critical to cellular function and it is a challenging statistical problem from the viewpoint of active matter physics [3–7]. *In vitro* experiments show that the distance traveled by cargoes substantially increases when the cargoes are transported by multiple motor proteins [8]. Various models have been developed that aim to explain how motors achieve long-range transport along microtubules [9–20].

Recently, it has been discovered that active cargo transport *in vivo* self-organizes into Lévy walks [21]. Lévy walks describe a wide spectrum of biological processes, such as T-cells migrating in brain tissue, collective behavior of swarming bacteria, and animals optimizing their search for sparse food [22]. Endosomal Lévy dynamics involves long flights in one direction due to the active movement along microtubules driven by multiple motors. When all active motors disengage, the cargo complexes detach from the microtubule and reattach to a new microtubule heading in another direction [21]. The travel distances have power-law distributions with diverging variances [22–26] that explains the anomalously long flights of cargo complex. In Ref. [21] the authors proposed the concept of memoryless self-reinforced directionality to demonstrate the emergence of Lévy walks.

However, the unanswered question remains: what is the precise mesoscopic kinetic mechanism of anomalous directional persistence? To answer this question, we performed *in vivo* experiments recording thousands of trajectories of intracellular lipid bound vesicles in live retinal pigment epithelium (RPE) cells and human bone osteosarcoma epithelial (U2OS) cells. We found similar results for both cell lines. Therefore, we report only results for RPE cells since a microscope with higher resolution was used to image them (see Sec. V for experimental details). In Fig. 1, we illustrate Lévy-like trajectories of vesicles inside RPE cells which consist of long persistent runs in one direction separated by rapid jiggling events when vesicles change direction.

In this paper we reveal a mechanism for anomalous directional persistence of cargoes in human cells: *the phenomenon of cumulative inertia*. Experimentally we found the longer a cargo moves along a microtubule, the less likely it will detach from it. Our data provides a direct measurement of the mesoscopic detachment rate as a decreasing function of the running time. We found that this time follows a heavy tailed Pareto distribution which leads to a Lévy-walk-like movement of cargoes. Since the observed detachment probability depends on how long the cargo has been moving, this active transport involves memory and it exhibits a typical non-Markovian behavior. Note that we are dealing with the memory which is not physically or chemically stored or retrieved and therefore energetically costs cells nothing.

II. EMPIRICAL SURVIVAL PROBABILITY, MESOSCOPIC DETACHMENT RATE, AND MEAN RESIDUAL TIME

One of our aims is to measure important statistical characteristics of cargo transport: the empirical survival probability of cargoes on the microtubule, the empirical mesoscopic detachment rate, and the mean residual time. The survival probability was estimated by using the nonparametric Kaplan-Meier estimator [27]. It is a common tool in many areas such as engineering to measure the time-to-failure of machine parts or medicine to determine time to death after an operation, time to recovery from an accident, and duration of pain relief [27]. We found a good agreement between the empirical survival probability Ψ and the heavy tailed Pareto distribution:

$$\Psi(\tau) = (1 + \tau/\tau_0)^{-\alpha}, \quad (1)$$

with the anomalous exponent $\alpha = 1.6 \pm 0.17$ and $\tau_0 = 0.17 \pm 0.1$ s up to 1–2 s (Fig. 2). The empirical mesoscopic detachment rate is also found to be a decreasing function of the flight time τ (inset Fig. 2). This means that the longer a cargo remains on a microtubule, the less likely it will detach from it (*the phenomenon of cumulative inertia*). Surprisingly, although having very different origin, a similar effect of

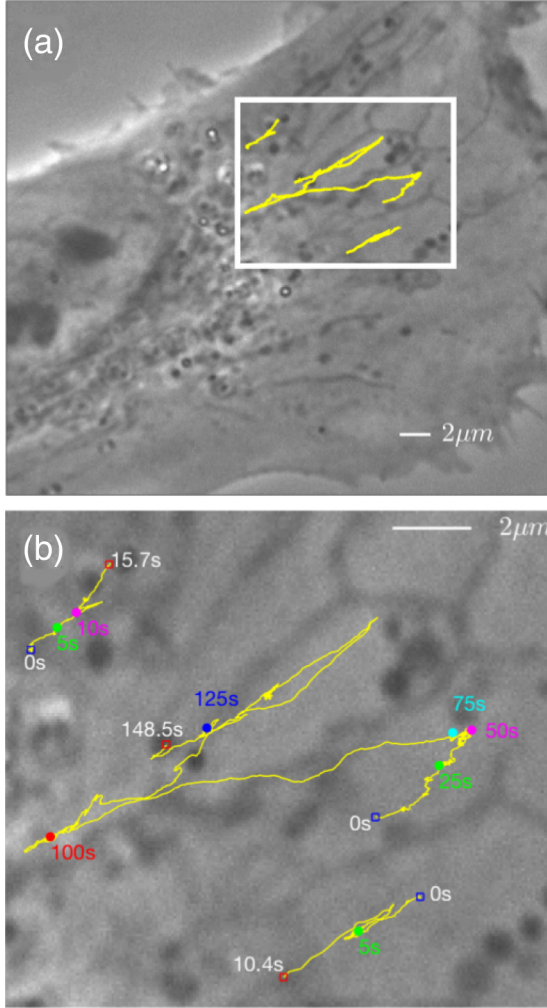


FIG. 1. Cargoes movement along microtubules visualized in a living RPE cell [panel (a)]. Panel (b) shows an enlargement of the boxed region in (a). Trajectories (yellow) consist of long flights in one direction and multiple turnings. Numbers indicate the time progress. The longest trajectory (148.5 s) in panel (b) consists of 900 flights (see Sec. V for the description of the segmentation procedure).

cumulative inertia is well studied and received revived interest in social and behavioral sciences [28,29]. The empirical mesoscopic detachment rate has a good fit with the rate inversely proportional to the flight time τ :

$$\gamma(\tau) = \alpha/(\tau + \tau_0), \quad (2)$$

with the same anomalous exponent $\alpha = 1.6 \pm 0.17$ and $\tau_0 = 0.17 \pm 0.1$ s. Note the relationship between $\Psi(\tau)$ and $\gamma(\tau)$: $\Psi(\tau) = \exp(-\int_0^\tau \gamma(t)dt)$. The time-dependent detachment rate $\gamma(\tau)$ has the following meaning: the product $\gamma(\tau)\Delta\tau$ defines the conditional probability of cargo detachment in the interval $(\tau, \tau + \Delta\tau)$ given that it has moved along the microtubule in the time interval $(0, \tau)$. For memoryless cargoes this rate will be constant and will not depend on how long the cargo has moved before. It is well known that the empirical rate is notoriously difficult to estimate [27] since it contains the derivative of the empirical survival function. Therefore, the empirical survival probability (which is an

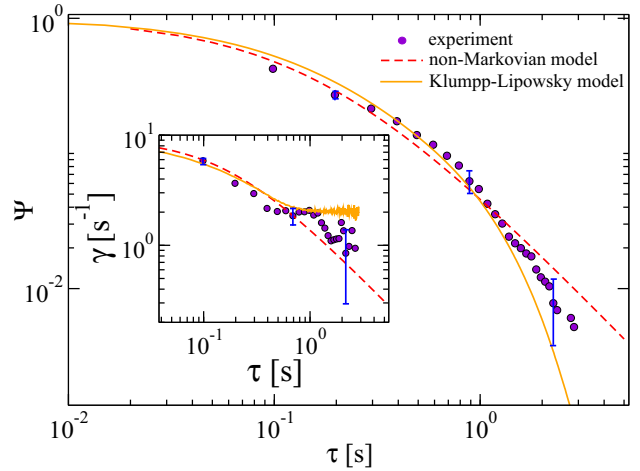


FIG. 2. Experimentally determined survival function $\Psi(\tau)$ (dots) as a function of time τ decays as a power law on intermediate time scale with anomalous exponent $\alpha = 1.6 \pm 0.17$ and a time-scale parameter $\tau_0 = 0.17 \pm 0.1$ s. The errors were calculated with the Greenwood formula for the nonparametric Kaplan-Meier estimator [27]. The red dashed curve is a power-law fit Eq. (1) with the same α and τ_0 . The orange solid curve is the survival function obtained in numerical simulations of the Klumpp-Lipowsky model of the cargo dynamics with six kinesin and six dynein motors. Details of simulations are given in Sec. VI. Inset: corresponding empirical mesoscopic detachment rate function $\gamma(\tau)$ (dots) as a function of time is inversely proportional to τ , Eq. (2), on intermediate time scales (red dashed curve) with the same α and τ_0 as in the main figure. The orange solid curve is the rate function obtained in numerical simulations.

integral quantity) has a smoother behavior compared to the empirical mesoscopic detachment rate function (Fig. 2).

The value of experimental exponent $\alpha = 1.6 \pm 0.17$ falls in the interval $1 < \alpha < 2$. This is an extraordinary finding since it shows that the survival function has finite mean, $\langle T \rangle = \int_0^\infty \tau \Psi(\tau)d\tau$, but divergent second moment [22]. Specifically the lack of the second moment leads to the emergence of the Lévy walklike trajectories of vesicles (Fig. 1). Such trajectories exhibit sub-ballistic superdiffusive behavior. We also obtain a good power-law fit with the anomalous exponent ($\alpha \simeq 1.5 \pm 0.17$) for the probability density of flight lengths (Fig. 3), which confirms the Lévy walk nature of the vesicles motion. The speed v of each flight was assumed to be constant. The probability density of flight length is obtained from the survival function as

$$f(L) = -\Psi'(L/v)/v, \quad (3)$$

where $\Psi'(z) = d\Psi(z)/dz$. In Fig. 3 the distribution of flight velocities is also shown.

If the cargo has survived on the microtubule up to time t , how much longer is it expected to move (survive) along the microtubule? This time is called the mean residual time $\tilde{T}(t)$. $\tilde{T}(t)$ is another important quantitative measure of cumulative inertia. From *in vivo* experiments we found that $\tilde{T}(t)$ increases linearly in time t already traveled; see Fig. 4. The longer the cargo remains on the microtubule, the larger the mean residual time, so the inertia is accumulated. This behavior is drastically

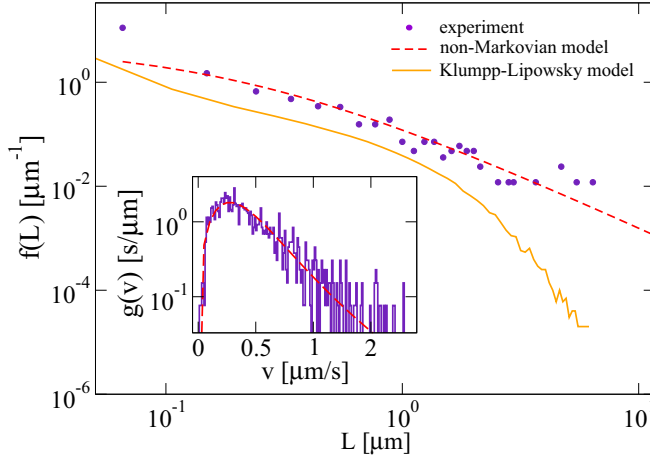


FIG. 3. Main panel: the experimental flight length probability density $f(L)$ (blue dots) fitted with Eq. (3) (red dashed curve) with $\alpha = 1.5 \pm 0.17$, $\tau_0 = 0.33 \pm 0.1$ s, and the average speed of the cargo $v = 0.8 \mu\text{m}/\text{s}$. The flight length distribution obtained in numerical simulations of the cargo dynamics using the Klumpp-Lipowsky model with six dynein and six kinesin motors (orange solid curve) decays exponentially for $L > 1 \mu\text{m}$. Parameters of the simulations are given in Sec. VI. The inset shows the distribution of experimental flight speed $g(v)$ (blue solid curve) approximated with the Burr density (red dashed curve) with parameters $\tilde{\gamma} = 0.57 \pm 0.07$, $\tilde{c} = 2.09 \pm 0.09$, and $\tilde{k} = 2.00 \pm 0.34$. The average speed of the cargo is $v = 0.8 \mu\text{m}/\text{s}$.

different to memoryless systems where $\bar{T}(t)$ is constant and does not depend on the prehistory. The data can be well explained by the conditional survival function for a random attachment time T , $\Psi_c(t, \tau) = \Pr\{T > t + \tau | T > t\}$. In our case,

$$\Psi_c(t, \tau) = \frac{\Psi(t + \tau)}{\Psi(t)} = \left(\frac{\tau_0 + t}{\tau_0 + t + \tau} \right)^\alpha \quad (4)$$

is an increasing function of time t already spent on the microtubule for a fixed τ . The behavior of $\Psi_c(t, \tau)$ is illustrated in the inset of Fig. 4. The mean residual time $\bar{T}(t)$ can be obtained as [30]

$$\bar{T}(t) = \int_0^\infty \Psi_c(t, \tau) d\tau = \frac{\tau_0 + t}{\alpha - 1}. \quad (5)$$

We found a good agreement between experimental mean residual time $\bar{T}(t)$ and Eq. (5) with $\tau_0 = 0.24 \pm 0.1$ and the anomalous exponent $\alpha = 1.8 \pm 0.17$, Fig. 4. Notice that the values of anomalous exponents obtained by fitting experimental data $\alpha = 1.6 \pm 0.17$ in Fig. 2, $\alpha = 1.5 \pm 0.17$ in Fig. 3, and $\alpha = 1.8 \pm 0.17$ in Fig. 4 agree with each other within the error bars. This cumulative inertia with $1 < \alpha < 2$ explains the dramatic increases of the traveled distance typical for Lévy walk. Since this is a non-Markovian effect with memory, our explanation of anomalous long distance transport is completely different from the idea of memoryless self-reinforced directionality [21] when the probability $P(L)$ of traveling in some direction grows with the distance L already traveled. This probability can be obtained in terms of the conditional survival function $\Psi_c(t, \tau)$ as $P(L) = \Psi_c(L/v, \tau)$.

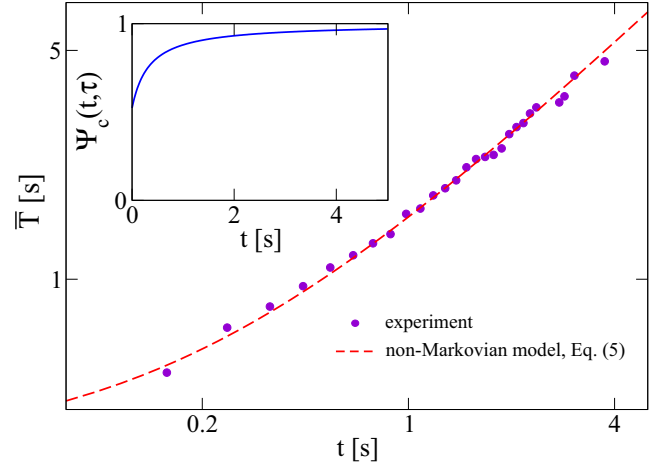


FIG. 4. Main panel: the experimental mean residual time \bar{T} of flights (blue dots) linearly increases (notice logarithmic scales on both the horizontal and vertical axes) with the time t already traveled. The theoretical prediction Eq. (5) with parameters $\tau_0 = 0.24 \pm 0.1$ s and $\alpha = 1.8 \pm 0.17$ (red dashed curve) is in good agreement with the experiment. Inset: illustration of the increasing conditional survival function $\Psi_c(t, \tau)$ given by Eq. (4) with $\tau_0 = 0.2$ s, $\alpha = 1.8$, and $\tau = 0.1$ s.

III. MICROSCOPIC MECHANISM FOR THE EMERGENCE OF THE DECREASING MESOSCOPIC DETACHMENT RATE

The question arises: what is the microscopic mechanism of the decreasing mesoscopic detachment rate $\gamma(\tau)$? A first insight could be obtained from a classical microscopic Klumpp-Lipowsky model [9]. Note that the authors of Ref. [9] did not consider this time-dependent rate. Instead, they found the constant effective unbinding rate.

Consider the cargo which is pulled by multiple motors. We assume that initially the cargo attaches to the microtubule with a single motor. As the cargo moves along the microtubule, the number of engaged motors $N(t)$ varies from 1 to \bar{N} . Motors attach to the microtubule and detach from it with effective microscopic rates π_n and ϵ_n (n is the number of engaged motors). We define the random detachment time T as the time when all active motors together with the cargo detach from the microtubule. In other words we have a random walk in the space of the number of engaged motors. In order to obtain the effective detachment rate $\gamma(\tau)$, one can define the survival function $\Psi(\tau)$ of the cargo to remain on the microtubule as the probability $\Psi(\tau) = \Pr\{T > \tau\} = 1 - \Pr\{N(\tau) = 0 | N(0) = 1\}$ [9]. The effective detachment rate is defined as [31]

$$\gamma(\tau) = -\Psi'(\tau)/\Psi(\tau). \quad (6)$$

The function $\Psi(\tau)$ can be written in terms of the probability distribution of the first passage time T from the cargo state with one engaged motor at time zero to the cargo state with zero engaged motors:

$$F(\tau) = \Pr\{T < \tau\} \quad (7)$$

as

$$\Psi(\tau) = 1 - F(\tau). \quad (8)$$

To find the distribution function $F(\tau)$ one can introduce the transition probability [9]

$$P_{n,0}(\tau) = \Pr\{N(\tau) = 0 | N(0) = n\}. \quad (9)$$

Define $F(\tau)$ as

$$F(\tau) = P_{1,0}(\tau), \quad (10)$$

where $P_{1,0}(\tau)$ is the transition probability from the cargo state with one engaged motor to the state with zero engaged motors. $P_{n,0}(\tau)$ obey the system of the backward Kolmogorov equations [31]:

$$\frac{dP_{n,0}(t)}{dt} = -(\varepsilon_n + \pi_n)P_{n,0}(t) + \varepsilon_n P_{n-1,0}(t) + \pi_n P_{n+1,0}(t), \quad (11)$$

with the initial conditions $P_{n,0}(0) = 0$ for $2 \leq n \leq \bar{N}$ and $P_{0,0}(t) = 1$ ($n = 0$ is the absorbing state). Here ε_n and π_n are the unbinding and binding rates. One can solve these equations and find the transition probability $P_{1,0}(\tau)$. It follows from Eqs. (6) and (8) that the effective detachment rate is

$$\gamma(\tau) = \frac{P'_{1,0}(\tau)}{1 - P_{1,0}(\tau)}. \quad (12)$$

This mesoscopic detachment rate is essentially different from the effective constant unbinding rate obtained within the Klumpp-Lipowsky model in Ref. [9] from equilibrium conditions. Our purpose is to show that the rate $\gamma(\tau)$ is a decreasing function of the running time τ . It means that the longer a cargo moves along the microtubule, the smaller is the probability that it will detach and switch the direction in the next time interval (a cumulative inertia effect). Numerical modeling confirms that γ is a decreasing function of τ on a certain time scale (see the orange solid curve in the inset of Fig. 2).

In vitro experimental data indicates that adding just one extra motor increases cargo run lengths by at least one order of magnitude compared to the distance traveled by a single motor [8]. To understand intuitively the reason why $\gamma(\tau)$ decreases with the flight time τ , consider the first event of attachment of a cargo complex with one motor. Initially the rate $\gamma(0) = \varepsilon_1$. Note that this defines the microscopic time scale $1/\varepsilon_1$. In turn, the mesoscopic time scale is given by $\langle T \rangle = \int_0^\infty \tau \Psi(\tau) d\tau$, $\langle T \rangle \gg 1/\varepsilon_1$. If the second motor attaches before the first motor detaches, the load is shared between two motors and the detachment rate ε_2 decreases, $\varepsilon_2 < \varepsilon_1$. As a result of this stochastic dynamics, the number of participating motors increases and therefore the detachment probability of the cargo decreases with the flight time. Cumulative inertia occurs due to multiple attachment and reattachment of motors before the cargo finally detaches from the microtubule. This leads to a dramatic increase of the traveled distance due to the directional persistence [8].

We consider the cargo pulled by two motors $\bar{N} = 2$ and show how the essential improvement of travel distance occurs. The backward Kolmogorov equations (11) take the form

$$\frac{dP_{2,0}(t)}{dt} = -\varepsilon_2 P_{2,0}(t) + \varepsilon_2 P_{1,0}(t), \quad (13)$$

$$\frac{dP_{1,0}(t)}{dt} = -(\pi_1 + \varepsilon_1)P_{1,0}(t) + \pi_1 P_{2,0}(t) + \varepsilon_1, \quad (14)$$

since $\pi_2 = 0$. Solving the above equations with the initial conditions $P_{1,0}(0) = P_{2,0}(0) = 0$, we find the cargo survival function $\Psi(t) = 1 - P_{1,0}(t)$:

$$\Psi(t) = p_1 e^{-k_1 t} + p_2 e^{-k_2 t}, \quad (15)$$

where

$$p_1 = \frac{\varepsilon_1}{k_2} \left(\frac{k_2 - \varepsilon_2}{k_2 - k_1} \right), \quad p_2 = \frac{\varepsilon_1}{k_1} \left(\frac{\varepsilon_2 - k_1}{k_2 - k_1} \right). \quad (16)$$

Here two real eigenvalues k_1 and k_2 ($k_1 < k_2$) are the solution of the quadratic equation

$$k^2 - (\pi_1 + \varepsilon_1 + \varepsilon_2)k + \varepsilon_1 \varepsilon_2 = 0. \quad (17)$$

Since

$$p_1 + p_2 = 1, \quad (18)$$

the survival function (15) has an interesting probabilistic interpretation as long as $\varepsilon_2 - k_1 > 0$ and $k_2 - \varepsilon_2 > 0$ (both p_1 and p_2 are positive). The cargo movement can be interpreted as one that involves a mixed population of two motors with different properties. The first motor has a probability p_1 to be engaged and it has the exponential density of dwelling time with the rate k_1 . p_2 is the probability of engagement for the second type of motor with the effective detachment rate k_2 . In this case the rate $\gamma(\tau)$ defined by (12) is *always* a decreasing function of running time τ :

$$\gamma(\tau) = \frac{p_1 k_1 e^{-k_1 \tau} + p_2 k_2 e^{-k_2 \tau}}{p_1 e^{-k_1 \tau} + p_2 e^{-k_2 \tau}}. \quad (19)$$

This explains the dramatic increase of running length of a cargo with two motors and non-Markovian nature of cargo movement. The detachment rate $\gamma(\tau)$ takes the maximum value at $\tau = 0$:

$$\gamma(0) = p_1 k_1 + p_2 k_2 = \varepsilon_1. \quad (20)$$

In the long-time limit, the detachment rate $\gamma(\tau)$ tends to the constant value k_1 such that $k_1 < \varepsilon_1$. This explains the dramatic increase of running length of a cargo with two motors and the non-Markovian nature of cargo movement. Our numerical results support this idea and show a decreasing detachment rate γ (inset Fig. 2). Note that the empirical power-law survival function can be approximated with the survival function in the form of the linear combination of exponents corresponding to the Klumpp-Lipowsky model (Fig. 2).

The survival function Eq. (15) has an interesting biological interpretation. The cargo movement can be viewed as one that involves a mixed population of two motors with different properties. If we extend this idea for a heterogeneous population of motors for which the rates k are gamma distributed with the probability density function $f(k) = \tau_0 k^{\alpha-1} e^{-\tau_0 k} / \Gamma(\alpha)$, the effective survival function

takes the form $\Psi(\tau) = \int_0^\infty e^{-k\tau} f(k) dk = (1 + \tau/\tau_0)^{-\alpha}$ consistent with Eq. (1).

IV. NON-MARKOVIAN DYNAMICS OF CARGO: SUPERDIFFUSION

Our next aim is to provide a theoretical link between the empirical mesoscopic detachment rate and the experimental Lévy-walk-like trajectories. The mesoscopic detachment rate Eq. (2) with the anomalous exponent $1 < \alpha < 2$ applied in Eq. (21) allows us to explain the emergence of Lévy walk as a result of anomalous cumulative inertia phenomena. We obtain the mean-squared displacement (MSD) which exhibits sub-ballistic superdiffusive behavior $\langle \mathbf{x}^2(t) \rangle \sim t^{3-\alpha}$. For Lévy walks with $1 < \alpha < 2$ the ensemble and time-averaged MSDs differ only by a factor of $1/(\alpha - 1)$ [32–34].

We define the probability density function $\xi(t, \mathbf{x}, \varphi, \tau)$ which gives the probability to find a cargo at point $\mathbf{x} = (x, y)$ at time t that moves with the speed v in the direction $\theta = (\cos \varphi, \sin \varphi)$ and having started the move a time τ ago. Here φ is the angle between the direction of movement θ and the x axis. We assume that as long as the cargo detaches from the microtubule it reattaches to another microtubule and thereby changes the direction of movement. The governing equation for $\xi(t, \mathbf{x}, \varphi, \tau)$ takes the form [35]

$$\frac{\partial \xi}{\partial t} + v\theta \cdot \nabla \xi + \frac{\partial \xi}{\partial \tau} = -\gamma(\tau)\xi, \quad (21)$$

with the boundary condition

$$\xi(t, \mathbf{x}, \varphi, 0) = \int_0^t \gamma(\tau) \int_{-\pi}^{\pi} R(\varphi - \varphi') \xi(t, \mathbf{x}, \varphi', \tau) d\varphi' d\tau, \quad (22)$$

where $R(\varphi - \varphi')$ is the probability density of the re-orientation from φ' to φ such that $\int_{-\pi}^{\pi} R(u) du = 1$. In Ref. [21] the flights were statistically isotropic with $R(u) = 1/2\pi$. In our experiments, we observe quasi one-dimensional trajectories (Fig. 1) for which the angle takes only two values [36].

The aim of this section is to obtain the non-Markovian master equation for the probability density:

$$p(t, \mathbf{x}, \varphi) = \int_0^t \xi(t, \mathbf{x}, \varphi, \tau) d\tau, \quad (23)$$

where the ξ is the structural density. We assume that at the initial time $t = 0$ cargo has a zero running time

$$\xi(t, \mathbf{x}, \varphi, 0) = p^0(t, \mathbf{x}, \varphi) \delta(\tau), \quad (24)$$

where $p^0(t, \mathbf{x}, \varphi)$ is the initial density. The density $p(t, \mathbf{x}, \varphi)$ can be found by differentiating (23) with respect to time t :

$$\frac{\partial p}{\partial t} + v\theta \cdot \nabla p = -i(t, \mathbf{x}, \varphi) + j(t, \mathbf{x}, \varphi), \quad (25)$$

where v is the cargo speed and $\theta = [\cos(\varphi), \sin(\varphi)]$ is the direction of the cargo's movement. The switching terms are

$$i(t, \mathbf{x}, \varphi) = \int_0^t \gamma(\tau) \xi(t, \mathbf{x}, \varphi, \tau) d\tau, \quad (26)$$

$$j(t, \mathbf{x}, \varphi) = \xi(t, \mathbf{x}, \varphi, 0)$$

$$= \int_0^t \int_{-\pi}^{\pi} R(\varphi - \varphi') \gamma(\tau) \xi(t, \mathbf{x}, \varphi', \tau) d\varphi' d\tau. \quad (27)$$

By using the method of characteristics we find for $\tau < t$:

$$\xi(t, \mathbf{x}, \varphi, \tau) = \xi(t - \tau, \mathbf{x} - v\theta\tau, \varphi, 0) e^{-\int_0^{\tau} \gamma(s) ds}. \quad (28)$$

The exponential factor in the above formula is the survival function:

$$\Psi(t) = e^{-\int_0^t \gamma(s) ds}. \quad (29)$$

To obtain $i(t, \mathbf{x}, \varphi)$, we use the Fourier-Laplace transform:

$$\hat{i}(s, \mathbf{k}, \varphi) = \int_{\mathbb{R}^2} \int_0^\infty i(t, \mathbf{x}, \varphi) e^{i\mathbf{k}\cdot\mathbf{x}-st} dt d\mathbf{x}, \quad (30)$$

$$\hat{p}(s, \mathbf{k}, \varphi) = \int_{\mathbb{R}^2} \int_0^\infty p(t, \mathbf{x}, \varphi) e^{i\mathbf{k}\cdot\mathbf{x}-st} dt d\mathbf{x}. \quad (31)$$

We find

$$\hat{i}(s, \mathbf{k}, \varphi) = \tilde{K}(s - iv\mathbf{k} \cdot \theta) \hat{p}(s, \mathbf{k}, \varphi), \quad (32)$$

where $\tilde{K}(s) = \tilde{\psi}(s)/\tilde{\Psi}(s)$. Finally we obtain the expressions for the switching terms:

$$i(t, \mathbf{x}, \varphi) = \int_0^t K(s) p(t - s, \mathbf{x} - v\theta s, \varphi) ds, \quad (33)$$

$$j(t, \mathbf{x}, \varphi) = \int_{-\pi}^{\pi} R(\varphi - \varphi') i(t, \mathbf{x}, \varphi') d\varphi'. \quad (34)$$

The main advantage of the present derivation is that it can be easily extended for the nonlinear case.

Superdiffusive equations can be obtained for the case when the detachment rate $\gamma(\tau)$ can be approximated by the following rate:

$$\gamma(\tau) = \frac{\alpha}{\tau_0 + \tau}, \quad 1 < \alpha < 2. \quad (35)$$

The rate (35) leads to a power-law (Pareto) survival function:

$$\Psi(\tau) = \left[\frac{\tau_0}{\tau_0 + \tau} \right]^\alpha \quad (36)$$

and corresponding running time PDF:

$$\psi(\tau) = \frac{\alpha \tau_0^\alpha}{(\tau_0 + \tau)^{1+\alpha}}. \quad (37)$$

The Laplace transform can be written in terms of the incomplete gamma function $\Gamma(a, b) = \int_b^\infty t^{a-1} e^{-t} dt$ as

$$\tilde{\psi}(s) = \alpha(\tau_0 s)^\alpha e^{\tau_0 s} \Gamma(-\alpha, \tau_0 s). \quad (38)$$

In the long-time limit as $s \rightarrow 0$, we have

$$\Gamma(-\alpha, \tau_0 s) = -\frac{\Gamma(1 - \alpha)}{\alpha} + (\tau_0 s)^{-\alpha} \alpha^{-1} + \frac{(\tau_0 s)^{1-\alpha}}{1 - \alpha} + \dots \quad (39)$$

For $1 < \alpha < 2$, using $\Gamma(-\alpha) = \frac{\Gamma(2-\alpha)}{\alpha(\alpha-1)}$ we obtain

$$\tilde{\psi}(s) \simeq 1 - \frac{\tau_0 s}{\alpha - 1} + \frac{\Gamma(2 - \alpha)(\tau_0 s)^\alpha}{(\alpha - 1)}, \quad s \rightarrow 0 \quad (40)$$

or

$$\tilde{\psi}(s) \simeq 1 - \bar{T}s + \Gamma(2 - \alpha)\tau_0^{\alpha-1}\bar{T}s^\alpha, \quad (41)$$

where $\bar{T} = \tau_0(\alpha - 1)^{-1}$ is the mean value of the random running time T . Then

$$\tilde{K}(s) = \frac{s\tilde{\psi}(s)}{1 - \tilde{\psi}(s)} \simeq \frac{1}{\bar{T}}(1 + \Gamma(2 - \alpha)(\tau_0 s)^{\alpha-1})$$

as $s \rightarrow 0$. Using (32) we write the Fourier-Laplace transform of $i(t, \mathbf{x}, \varphi)$ as

$$\hat{i} = \frac{1}{\bar{T}}(1 + \Gamma(2 - \alpha)\tau_0^{\alpha-1}(s - iv\mathbf{k} \cdot \boldsymbol{\theta})^{\alpha-1})\hat{p}. \quad (42)$$

The switching term $i(t, \mathbf{x}, \varphi)$ can be written as [37]

$$i = \frac{1}{\bar{T}} \left[1 + \Gamma(2 - \alpha)\tau_0^{\alpha-1} \left(\frac{\partial}{\partial t} - v\boldsymbol{\theta} \cdot \nabla \right)^{\alpha-1} \right] p, \quad (43)$$

where the fractional material derivative $(\frac{\partial}{\partial t} - v\boldsymbol{\theta} \cdot \nabla)^{\alpha-1}$ of order $\alpha - 1$ is defined by their Fourier-Laplace transforms

$$\mathcal{L}\mathcal{F} \left\{ \left(\frac{\partial}{\partial t} - v\boldsymbol{\theta} \cdot \nabla \right)^{\alpha-1} p \right\} = (s - iv\mathbf{k} \cdot \boldsymbol{\theta})^{\alpha-1} \tilde{p}(s, \mathbf{k}, \varphi). \quad (44)$$

Taking the Laplace transform of Eq. (25) and substituting the Laplace transform of Eq. (43) into it [using Eq. (34)] and Eq. (42), we solve the equation for \tilde{p} . Then, differentiating \tilde{p} twice and taking the inverse Laplace transform, we find the mean-squared displacement $\langle \mathbf{x}^2(t) \rangle$. For the isotropic case with the uniform angle distribution $R(u) = 1/2\pi$ (Granick data [21]) or quasi-one-dimensional trajectories (our data) the mean-squared displacement exhibits sub-ballistic super-diffusive behavior

$$\langle \mathbf{x}^2(t) \rangle \sim t^{3-\alpha}, \quad 1 < \alpha < 2. \quad (45)$$

In Fig. 5 we show the time-averaged mean-squared displacement calculated along single experimental trajectories (corrected for the drift) which was also averaged over many trajectories. A clear power-law behavior with the exponent 1.51 ± 0.17 is found which is consistent with the Lévy walk behavior and with the behavior of the detachment rate and survival functions.

V. EXPERIMENTAL METHODS AND ANALYSIS OF TRAJECTORIES

Intracellular vesicles of U2OS (human bone osteosarcoma epithelial) and RPE (retinal pigment epithelial) cells were imaged using phase contrast microscopy and tracked with Polyparticle Tracker software [38]. The cells were grown in DMEM (Sigma Life Science) and 10% FBS (HyClone) and incubated for 48 h at 37 °C in 8% CO₂ on 35 mm glass-bottomed Ibidi dishes. Before imaging, the cells were moved to a live-imaging media. The live-cell imaging was done using an inverted Olympus IX71 with an Olympus 100 × /1.35 oil

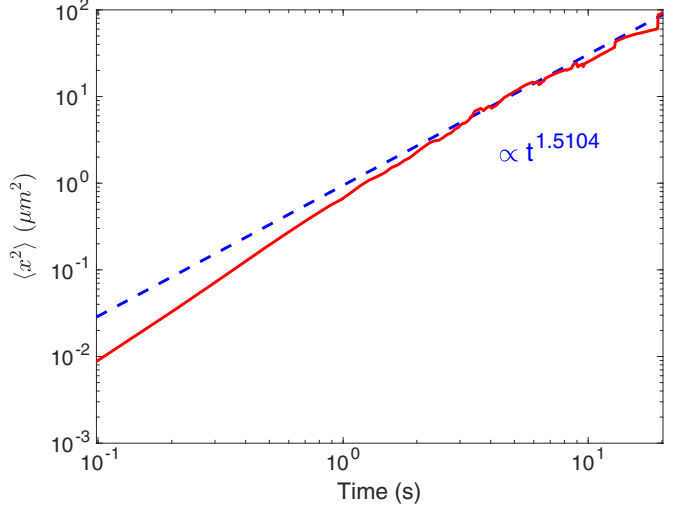


FIG. 5. Anomalous behavior of the time-averaged mean-squared displacement for experimental trajectories in RPE cell (corrected for the drift and averaged over many trajectories). The dashed curve represents the power-law function with the exponent 1.5 ± 0.17 .

PH3 objective and 1.6× zoom. A QuantEM 512SC CCD Camera and Cool LED pE-100 light source was used for the continuous imaging of U2OS cells and a CoolSNAP HQ2 was used for the RPE cells. The video was taken with 30 ms or 98.5 ms exposure times, while the cells were kept at 37° in atmospheric CO₂ levels.

After tracking each vesicle's path, only those with maximum displacement greater than 1 μm were chosen. Our aim was to filter those vesicles that are involved in active transport along microtubules. For this reason, we use the time-averaged mean-square displacements (MSDs) for single vesicle trajectories:

$$\langle \mathbf{x}^2(m\delta t) \rangle = \frac{1}{N-m} \sum_{i=1}^{N-m} [\mathbf{x}(t_i + m\delta t) - \mathbf{x}(t_i)]^2, \quad (46)$$

where $\mathbf{x} = (x, y)$ is the vesicle coordinate and the video contains N snapshots at increments of δt . The total time of a data set is then $T = (N - 1)\delta t$ and $m = 1, 2, \dots, N - 1$. Lag times are defined as the set of possible $m\delta t$ within the data set. Trajectories with mean-square displacements (MSDs) close to t^2 (active transport) were analyzed [39]. The lower limit for the MSD was balanced between sufficient statistics to produce good fits and its proximity to t^2 proportionality. These criteria were applied to restrict analysis due to the noisy background of vesicles engaging in motion differing from directed transport on microtubules.

To measure the turning times of the vesicles, an angular threshold method was used in conjunction with a distance threshold. In a set of N points, there will be $N - 2$ angles characterizing the direction of the path and for three arbitrary data points, $i, i + 1$, and $i + 2$, the angle deviation of the path was calculated by [19]

$$\theta_{i+1} = \arccos \left(\frac{\mathbf{x}_{i \rightarrow (i+1)} \cdot \mathbf{x}_{(i+1) \rightarrow (i+2)}}{|\mathbf{x}_{i \rightarrow (i+1)}| |\mathbf{x}_{(i+1) \rightarrow (i+2)}|} \right). \quad (47)$$

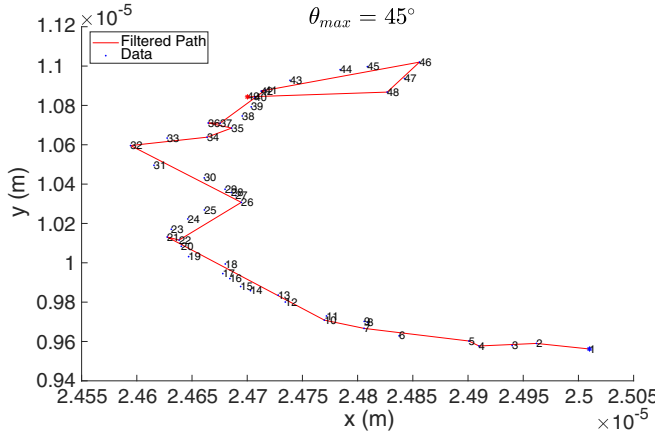


FIG. 6. Position of a tracked particle path segmented using $\theta_{\max} = 45^\circ$. Blue dots with frame numbers mark the path. The red line indicates the new segmented path. The blue star marks the start position and the red star marks the end position.

If $\theta_{i+1} > \theta_{\max}$, the path was deemed to have changed direction. Additionally, if the tracked vesicle had not moved greater than 10% of the length of a pixel, during the turn, the path was deemed to not have changed direction. This threshold was to ensure that stationary or completely detached vesicles, that move diffusively, do not add false runs to the statistics. In order to ensure results were not dependent on the arbitrary value of θ_{\max} , a set of threshold angles were tested ranging from 5° to 90° in 5° increments. We found $\theta_{\max} = 45^\circ$ to be optimal. With such an angular threshold, we have a good quality of the trajectory segmentation as shown in Fig. 6.

VI. NUMERICAL MODELING

In experimental trajectories we found retrograde (towards the cell center) and anterograde (away from the cell center) movement which suggests that vesicles are driven by both kinesins and dyneins. However, we observe no long pauses between retrograde and anterograde movement (Fig. 1) and conclude that it is unlikely that kinesins and dyneins were engaged in a tug of war [15,16]. Instead, changes of the direction could be triggered by some regulatory mechanism which remains poorly understood [17,18].

To model the multimotor cargo transport we consider two groups of kinesin and dynein motors. Only kinesins or dyneins are engaged in cargo movement at any time. There are some indications (although still debated in the literature) that motors are loaded on the cargo in pairs [40]. We suppose that there is an equal number of kinesins and dyneins. The groups can change after the number of engaged motors reaches zero and the cargo detaches from the microtubules. We assume that initially the cargo attaches to the microtubule with a single kinesin or dynein motor and moves along it pulled by $N(t)$ motors of one polarity. The number of engaged motors $N(t)$ varies from 1 to \bar{N} . The motors detach and reattach with rates ε_n and π_n . It is assumed that all motors equally share the external load.

The number of kinesins and dyneins decreases and increases with the rates ε_n and π_n given by [41]

$$\varepsilon_n = n\varepsilon e^{\frac{F_v}{nF_d}}, \quad \pi_n = \pi(\bar{N} - n), \quad (48)$$

where F_v is the force acting on the cargo which depends on its velocity v , F_d is the corresponding detachment force for kinesin or dynein, π is the binding constant for a single kinesin or dynein motor, and ε is their zero-load unbinding rate. The values of π , ε , and \bar{N} were adjusted to match the experimental data.

The cargo pulled by n motors has the velocity

$$v(F_v) = v \left(1 - \frac{F_v}{nF_s} \right), \quad (49)$$

where F_s is the motor stall force and v is the load-free velocity. The force F_v which is acting on the cargo of radius r due to viscous resistance also depends on the velocity of the cargo $F_v = 6\pi\eta rv$. Substituting this into the above expression and solving for the velocity, the consistent expression for the velocity is [41]

$$v(F_v) = \frac{v}{1 + (6\pi\eta rv)/(nF_s)}. \quad (50)$$

In our experiment, the typical radius of the lipid bound vesicles was $0.5 \mu\text{m}$. The cytoplasm is estimated to be 1000 times more viscous than the buffer [42], $\eta = 0.89 \text{ Pa s}$. Below we give the set of parameters used in simulations shown in Fig. 2 in the main text. We have used parameters for kinesins and dyneins from Ref. [43]. For kinesins: $v = 1 \mu\text{m/s}$, $\pi = 1 \text{ s}^{-1}$, $\varepsilon = 2 \text{ s}^{-1}$, $F_d = 4 \text{ pN}$, and $F_s = 5 \text{ pN}$. For dyneins: $v = 1 \mu\text{m/s}$, $\pi = 1 \text{ s}^{-1}$, $\varepsilon = 3 \text{ s}^{-1}$, $F_d = 0.87 \text{ pN}$, and $F_s = 1.25 \text{ pN}$.

VII. DISCUSSION AND CONCLUSION

In summary, we studied experimentally the non-Markovian anomalous multimotor intracellular transport of cargoes inside cells. We directly measured the mesoscopic detachment rate of cargoes from microtubules and demonstrated that the origin of the anomalous non-Markovian behavior is the cumulative inertia phenomenon. We provided evidence for this phenomenon in both bone and retina epithelial cells, but it is expected to occur in all cell types that use dyneins and kinesins to transport cargoes along microtubules. We proposed a mesoscopic model which explains the emergence of memory and non-Markovian behavior in the intracellular cargo transport on a mesoscopic scale. We also demonstrated how this non-Markovian behavior emerged from a Markovian memoryless dynamics of multiple motors on a microscopic scale. At the same time we note that the microscopic model is inconvenient since it has multiple parameters which require difficult fine-tuning. And, more importantly, almost all parameters in the microscopic model are unknown *in vivo*. There is no experimental technique to measure them. On the contrary, our mesoscopic model is computationally cheap and has only two parameters which we measure directly in the experiment. We believe that our model provides a complementary description of the intracellular transport on a mesoscopic scale that is better able to model the experimentally observed memory effects.

The impact of our work on the field of intracellular transport will be threefold: first, we experimentally show the non-Markovian nature of intracellular transport and memory effects on a mesoscopic scale. Secondly, our results settle the controversy in the field of intracellular transport (see the work of Granick *et al.* [21]) about memoryless Markovian dynamics on a microscopic scale and non-Markovian behavior and memory effects on a mesoscopic scale. Thirdly, with our work we are shifting the paradigm of how the single-particle tracking experiments could be analyzed by introducing several mesoscopic statistical quantities, such as the mesoscopic detachment rate, the survival function, and the mean residual time to remain on the microtubule. We believe that these quantities are better for a description of the long-time properties of intracellular transport than the traditionally used mean-squared displacements along single trajectories. What

is important is that we show that these quantities are experimentally measurable, can be predicted, and can be modeled in a self-consistent manner (improving our confidence in the robustness of our analysis). Improved non-Markovian modeling will lead to more accurate quantitative analysis of the kinetics of a huge range of active transport in cellular physiology. Such transport impacts on a vast range of cellular processes and their diseased states, e.g., motor neuron disease and cancer.

ACKNOWLEDGMENTS

S.F., N.K., T.A.W., and V.J.A. acknowledge financial support from EPSRC Grant No. EP/J019526/1. D.H. acknowledges funding from the Wellcome Trust, Grant No. 108867/Z/15/Z.

-
- [1] R. D. Vale, The molecular motor toolbox for intracellular transport, *Cell* **112**, 467 (2003).
 - [2] P. C. Bressloff, *Stochastic Processes in Cell Biology*, 4th ed. (Springer, New York, 2014).
 - [3] C. Loverdo, O. Benichou, M. Moreau, and R. Voituriez, Enhanced reaction kinetics in biological cells, *Nat. Phys.* **4**, 134 (2008).
 - [4] B. Wang, J. Kuo, and S. Granick, Bursts of Active Transport in Living Cells, *Phys. Rev. Lett.* **111**, 208102 (2013).
 - [5] P. K. Trong, J. Guck, and R. E. Goldstein, Coupling of Active Motion and Advection Shapes Intracellular Cargo Transport, *Phys. Rev. Lett.* **109**, 028104 (2012).
 - [6] C. P. Brangwynne, G. H. Koenderink, F. C. MacKintosh, and D. A. Weitz, Intracellular transport by active diffusion, *Trends Cell Biol.* **19**, 423 (2009).
 - [7] S. M. A. Tabei *et al.*, Intracellular transport of insulin granules is a subordinated random walk, *Proc. Natl. Acad. Sci. USA* **110**, 4911 (2013).
 - [8] M. Vershinin, B. C. Carter, D. S. Razafsky, S. J. King, and S. P. Gross, Multiple-motor based transport and its regulation by Tau, *Proc. Natl. Acad. Sci. USA* **104**, 87 (2007).
 - [9] S. Klumpp and R. Lipowsky, Cooperative cargo transport by several molecular motors, *Proc. Natl. Acad. Sci. USA* **102**, 17284 (2005).
 - [10] F. Berger, C. Keller, M. J. I. Müller, S. Klumpp, and R. Lipowsky, Co-operative transport of molecular motors, *Biochem. Soc. Trans.* **39**, 1211 (2011).
 - [11] F. Berger, C. Keller, S. Klumpp, and R. Lipowsky, Distinct Transport Regimes for Two Elastically Coupled Molecular Motors, *Phys. Rev. Lett.* **108**, 208101 (2012).
 - [12] P. C. Bressloff and J. M. Newby, Stochastic models of intracellular transport, *Rev. Mod. Phys.* **85**, 135 (2013).
 - [13] F. Jülicher, A. Ajdari, and J. Prost, Modeling molecular motors, *Rev. Mod. Phys.* **69**, 1269 (1997).
 - [14] A. B. Kolomeisky and M. E. Fisher, Molecular motors: a theorist's perspective, *Annu. Rev. Phys. Chem.* **58**, 675 (2007).
 - [15] M. A. Welte, S. P. Gross, M. Postner, S. M. Block, and E. F. Wieschaus, Developmental regulation of vesicle transport in *Drosophila* embryos: forces and kinetics, *Cell* **92**, 547 (1998).
 - [16] M. J. Müller, S. Klumpp, and R. Lipowsky, Tug-of-war as a cooperative mechanism for bidirectional cargo transport by molecular motors, *Proc. Natl. Acad. Sci. USA* **105**, 4609 (2008).
 - [17] C. Leidel, R. A. Longoria, F. M. Gutierrez, and G. T. Shubeita, Measuring molecular motor forces in vivo: Implications for tug-of-war models of bidirectional transport, *Biophys. J.* **103**, 492 (2012).
 - [18] W. O. Hancock, Bidirectional cargo transport: moving beyond tug of war, *Nat. Rev. Mol. Cell Biol.* **15**, 615 (2014).
 - [19] A. W. Harrison, D. A. Kenwright, T. A. Waigh, P. G. Woodman, and V. J. Allan, Modes of correlated angular motion in live cells across three distinct time scales, *Phys. Biol.* **10**, 036002 (2013).
 - [20] Q. Li, S. King, A. Gopinathan, and J. Xu, Quantitative determination of the probability of multiple-motor transport in bead-based assays, *Biophys. J.* **110**, 2720 (2016).
 - [21] K. Chen, B. Wang, and S. Granick, Memoryless self-reinforcing directionality in endosomal active transport within living cells, *Nat. Mater.* **14**, 589 (2015).
 - [22] V. Zaburdaev, S. Denisov, and J. Klafter, Lévy walks, *Rev. Mod. Phys.* **87**, 483 (2015).
 - [23] R. Metzler and J. Klafter, The restaurant at the end of the random walk: recent developments in the description of anomalous transport by fractional dynamics, *J. Phys. A: Math. Gen.* **37**, R161 (2004).
 - [24] E. Barkai, Y. Garini, and R. Metzler, Strange kinetics of single molecules in living cells, *Phys. Today* **65**, 29 (2012).
 - [25] F. Höfling and T. Franosch, Anomalous transport in the crowded world of biological cells, *Rep. Prog. Phys.* **76**, 046602 (2013).
 - [26] J. Klafter and I. M. Sokolov, *First Steps in Random Walks: from Tools to Applications* (Oxford University Press, Oxford, 2011).
 - [27] O. Aalen, Ø. Borgan, and H. Gjessing, *Survival and Event History Analysis: A Process Point of View* (Springer, New York, 2008).
 - [28] D. G. Morrison and D. C. Schmittlein, Jobs, strikes, and wars: Probability models for duration, *Organ. Behav. Hum. Perform.* **25**, 224 (1980).
 - [29] S. Fedotov and H. Stage, Anomalous Metapopulation Dynamics on Scale-Free Networks, *Phys. Rev. Lett.* **118**, 098301 (2017).

- [30] D. G. Morrison, On linearly increasing mean residual lifetimes, *J. Appl. Prob.* **15**, 617 (1978).
- [31] D. R. Cox and H. D. Miller, *The Theory of Stochastic Processes* (Methuen, London, 1965).
- [32] G. Zumofen and J. Klafter, Power spectra and random walks in intermittent chaotic systems, *Phys. D* **69**, 436 (1993).
- [33] D. Froemberg and E. Barkai, Time-averaged Einstein relation and fluctuating diffusivities for the Lévy walk, *Phys. Rev. E* **87**, 030104(R) (2013).
- [34] R. Metzler, J.-H. Jeon, A. G. Cherstvy, and E. Barkai, Anomalous diffusion models and their properties: non-stationarity, non-ergodicity, and ageing at the centenary of single particle tracking, *Phys. Chem. Chem. Phys.* **16**, 24128 (2014).
- [35] W. Alt, Biased random walk models for chemotaxis and related diffusion approximations, *J. Math. Biol.* **9**, 147 (1980).
- [36] S. Fedotov, Single integrodifferential wave equation for a Lévy walk, *Phys. Rev. E* **93**, 020101 (2016).
- [37] I. M. Sokolov and R. Metzler, Towards deterministic equations for Lévy walks: The fractional material derivative, *Phys. Rev. E* **67**, 010101(R) (2003).
- [38] S. S. Rogers, T. A. Waigh, X. Zhao, and J. R. Lu, Precise particle tracking against a complicated background: Polynomial fitting with Gaussian weight, *Phys. Biol.* **4**, 220 (2007).
- [39] D. Arcizet, B. Meier, E. Sackmann, J. O. Rádler, and D. Heinrich, Temporal Analysis of Active and Passive Transport in Living Cells, *Phys. Rev. Lett.* **101**, 248103 (2008).
- [40] D. St. Johnston, Counting motors by force, *Cell* **135**, 1000 (2008).
- [41] A. Kunwar and A. Mogilner, *Phys. Biol.* **7**, 016012 (2010).
- [42] K. Luby-Phelps, *Int. Rev. Cytol.* **192**, 189 (2000).
- [43] A. Kunwar *et al.*, Mechanical stochastic tug-of-war models cannot explain bidirectional lipid-droplet transport, *Proc. Natl. Acad. Sci. USA* **108**, 18960 (2011).